

Coexistence of superconducting and superionic states in lithium boron compounds under high pressure

Pei Zhou(周佩), Yuhang Li(李宇航), Junjie Wang(王俊杰), Qing Lu(鲁清), Yu Han(韩瑜), Chi Ding(丁驰), Yang Ni(倪洋), Xiaomeng Wang(王晓梦), and Jian Sun(孙建)

Citation: Chin. Phys. B, 2026, 35 (**5**): 056201. DOI: 10.1088/1674-1056/ae39d5
http://cpb.iphy.ac.cn; http://iopscience.iop.org/cpb

What follows is a list of articles you may be interested in

Dynamic mechanical response of polystyrene at high strain rates under uniaxial strain ramp loading

Xuping Zhang(张旭平), Fuli Tan(谭福利), Binqiang Luo(罗斌强), Guiji Wang(王桂吉), Jianheng Zhao(赵剑衡), and Chengwei Sun(孙承纬)

Chin. Phys. B, 2026, 35 (**4**): 046201. DOI: 10.1088/1674-1056/ae0637

Structural stability and properties of Li_2XN_6 (X = Be, Mg, Ca) ternary nitrides

Rui Wang(王睿), Cai-Zi Zhang(张才姿), Qi-Wen Jiang(蒋其雯), En-Yu Wang(王恩宇), Jie Wei(魏杰), and Hong-Yang Zhu(祝洪洋)

Chin. Phys. B, 2026, 35 (**3**): 036201. DOI: 10.1088/1674-1056/ae1f03

Theoretical investigation on the H sublattice in CaH_6 and energetic performance

Zhihong Huang(黄植泓), Nan Li(李楠), Jun Zhang(张俊), Xiuyuan Li(李修远), Zihuan Peng(彭梓桓), Chongwen Jiang(江崇文), and Changqing Jin(靳常青)

Chin. Phys. B, 2025, 34 (**8**): 086202. DOI: 10.1088/1674-1056/ade1c3

A novel metastable structure and superconductivity of hydrogen-rich compound CdH_6 under pressure

Yan Yan(闫岩), Chengao Jiang(蒋成澳), Wen Gao(高稳), Rui Chen(陈蕊), Xiaodong Yang(杨晓东), Runru Liu(刘润茹), Lihua Yang(杨丽华), and Lili Wang(王丽丽)

Chin. Phys. B, 2025, 34 (**8**): 086201. DOI: 10.1088/1674-1056/add902

Band gap engineering and vibrational properties of van der Waals semiconductor $ZnPSe_3$ under compression

Rouqiong Su(苏柔琼), Yuying Li(李玉莹), Chunhua Chen(陈春华), Yifang Yuan(袁亦方), and Haizhong Guo(郭海中)

Chin. Phys. B, 2025, 34 (**6**): 066205. DOI: 10.1088/1674-1056/adcaa2

SPECIAL TOPIC — Structures and properties of materials under high pressure

Coexistence of superconducting and superionic states in lithium boron compounds under high pressure

Pei Zhou(周佩)[1,†], Yuhang Li(李宇航)[1,†], Junjie Wang(王俊杰)[2], Qing Lu(鲁清)[2], Yu Han(韩瑜)[2], Chi Ding(丁驰)[2], Yang Ni(倪洋)[1], Xiaomeng Wang(王晓梦)[1,‡], and Jian Sun(孙建)[2,§]

[1] *School of Physics, Ningxia University, Yinchuan* 750021, *China*

[2] *National Laboratory of Solid State Microstructures, School of Physics and Collaborative Innovation Center of Advanced Microstructures, Nanjing University, Nanjing* 210093, *China*

(Received 2 December 2025; revised manuscript received 16 January 2026; accepted manuscript online 19 January 2026)

Lithium-based compounds with interstitial anionic electrons (IAEs) exhibit unique electronic properties, including superconductivity and superionic behavior. The intrinsic connection between these properties offers valuable insights and potential applications in materials science. In this study, we employed machine-learning-accelerated crystal structure prediction and first-principles calculations to investigate the phase stability of various Li−B systems under high pressures. Our results indicate that the known *R-3m* Li_6B compound is an electride. At 150 GPa, *R-3m* Li_6B exhibits a superconducting transition temperature of around 51 K and enters a superionic state at high temperatures. Additionally, a monoclinic compound, *C2/m* LiB_6, which is metastable at ambient pressure, was found. More interestingly, an unpredicted cage-like metallic boron allotrope termed *C2/m*-B_{12} can be obtained by removing Li from LiB_6. These findings open avenues for interdisciplinary research and highlight the potential of exotic boron allotropes in advanced device applications.

Keywords: high pressure, lithium-rich electrides, superconductivity, superionic behavior

PACS: 62.50.–p, 61.50.Ah, 71.20.–b, 74.25.–q

DOI: 10.1088/1674-1056/ae39d5 **CSTR:** 32038.14.CPB.ae39d5

1. Introduction

Among light elements, lithium and boron have attracted significant interest due to their intricate phase diagrams and electronic changes under extreme conditions. Over the past several decades of experimental and theoretical efforts, the phase diagram of lithium at pressures up to approximately 130 GPa has been established, revealing a series of solid-phase transitions with complex crystal structures: bcc $\xrightarrow{\sim 7\ \mathrm{GPa}}$ fcc $\xrightarrow{\sim 39\ \mathrm{GPa}}$ hR1 $\xrightarrow{\sim 42\ \mathrm{GPa}}$ cI16 $\xrightarrow{\sim 60\ \mathrm{GPa}}$ oc88 $\xrightarrow{\sim 70\ \mathrm{GPa}}$ oC40 $\xrightarrow{\sim 95\ \mathrm{GPa}}$ oC24.[1–6] These structural changes are accompanied by remarkable property transformations, including superconductivity,[7–9] electronic transitions,[10] electride phases,[11–14] and abnormal melting behaviors.[15–17]

Boron, on the other hand, is an element known for its fascinating chemical complexity, primarily due to its electron-deficient nature, which leads to distinctive bonding characteristics such as multi-center bonds. This unique behavior results in a diverse array of boron allotropes.[18–20] Studies have shown that boron readily forms compounds with various elements, displaying a wide range of physical and chemical properties.[21–24] A notable example is MgB_2, a new type of superconducting material with a unique dual-band structure, whose superconducting mechanism follows the Bardeen–Cooper–Schrieffer (BCS) electron–phonon coupling model.[21]

Electrides are a unique class of materials in which electrons act as anions, occupying empty spaces within the crystal lattice.[25] These interstitial anionic electrons (IAEs) endow electrides with properties suitable for a range of applications, including energy storage, catalysis, and use as strong reducing agents.[26–29] Recent research into the electronic properties of solid-state materials has highlighted the potential of electrides across various advanced applications, particularly due to the following categories of behavior: (i) Topological electrides. In these materials, the interstitial states may appear as occupied states located near the Fermi level, making them suitable for realizing the band inversion required for topological phases.[30] Electrides have thus been identified as promising materials for achieving topological phases, such as topological insulating phases in Cs_3O[31] and topological nodal-line semimetal phases in Y_2C.[32] (ii) Superconducting electrides. The coexistence of superconductivity and electride states has garnered considerable attention, especially in lithium-rich electrides.[33–38] Compounds such as Li_6P,[34] Li_5He_2[35] and $Li_{10}Ge$[38] exhibit interconnected IAEs that enhance their superconducting transition temperatures (T_c) to 39.3 K, 26 K,

[†]These authors contributed equally to this work.

[‡]Corresponding author. E-mail: xiaomengwang@nxu.edu.cn

[§]Corresponding author. E-mail: jiansun@nju.edu.cn

© 2026 Chinese Physical Society and IOP Publishing Ltd. All rights, including for text and data mining, AI training, and similar technologies, are reserved.

and 8.5 K at 270 GPa, 210 GPa, and 50 GPa, respectively, due to lithium's electron-donating nature. (iii) Electrides with superconducting and superionic behavior. The superionic state, a novel state of matter positioned between ordered crystalline states and disordered liquid or molten states, has attracted attention in earth and planetary science.[39–41] In recent years, many lithium-rich compounds,[42–47] such as Li–Al[42] systems, have demonstrated the simultaneous presence of superconductivity and superionicity under high pressure. An interesting question is whether compounds of Li and B will exhibit distinctly different properties when combined under high pressure.

2. Methods

We carried out variable-composition searches for Li–B compounds containing up to 50 atoms per unit cell at 50 GPa, 100 GPa, and 150 GPa using a machine-learning-accelerated crystal structure prediction method (MAGUS code).[48,49] The first-generation structures were randomly generated through a space-group method. In subsequent generations, 60% of the structures were randomly generated. The search was implemented for 50 generations, with each generation containing up to 50 structures. Structural relaxations and electronic property calculations were performed based on density functional theory within the Perdew–Burke–Ernzerhof (PBE) exchange–correlation functional[50] in the framework of the projector-augmented-wave (PAW) method[51] for ionic potentials, as implemented in the Vienna *ab initio* simulation package (VASP).[52] The valence electron configurations used were $1s^2 2s^1$ for Li and $2s^2 2p^1$ for B. The energy cutoff of the plane-wave basis was 800 eV, and the Brillouin zone was sampled by a *k*-point mesh with a reciprocal-space resolution of $2\pi \times 0.025$ Å^{-1}. The electron–phonon coupling and superconductivity calculations were performed using density functional perturbation theory, as implemented in the QUANTUM ESPRESSO code.[53] The kinetic-energy cutoff and the charge-density cutoff of the plane-wave basis were chosen to be 600 Ry and 150 Ry, respectively. Self-consistent electron density and electron–phonon coupling were calculated by employing $20 \times 20 \times 20$, $24 \times 24 \times 12$, and $18 \times 18 \times 18$ *k*-meshes and $4 \times 4 \times 4$, $4 \times 4 \times 2$, and $3 \times 3 \times 3$ *q*-meshes for Li_6B, LiB_6, and B_{12}, respectively. *Ab initio* molecular dynamics (AIMD)[54] simulations were performed in the NVT ensemble using a Nosé–Hoover thermostat,[55] with a time step of 1 fs and a supercell containing 168 atoms for Li_6B. An empty sphere with a Wigner–Seitz radius of 1.20 Å was used to obtain the projected density of states (DOS) on the interstitial position ("*X*" site).

3. Results

3.1. Crystal structure under high pressure

We constructed thermodynamic convex hulls for the Li–B binary system under 50 GPa, 100 GPa, and 150 GPa (Fig. 1(a)). The stability of each Li–B compound was evaluated by calculating the formation enthalpies relative to their decomposition into the most stable solid phases of Li and B at each pressure. Our results are consistent with previous studies,[56,57] successfully reproducing known stable Li–B compounds, including *R-3m* LiB, $P6_3/mmc$ LiB, *Fd-3m* LiB, *R-3m* Li_3B_2, *Cmcm* Li_2B, *C2/m* Li_4B, *R-3m* Li_6B, *C2/m* LiB_3, *Pnma* LiB_3, and *I4/mmm* LiB_4. Interestingly, we also predict a new metastable compound, LiB_6, which lies approximately 80 meV/atom above the convex hull at 100 GPa and remains dynamically stable even at ambient pressure. Zero-point energy (ZPE) was considered in evaluating the energetic stability of Li–B phases. While ZPE may influence phase stability, its effect was found to be relatively minor. We further established a pressure–composition phase diagram, highlighting the dynamical stability ranges of both stable and metastable Li–B phases (Fig. 1(b)). In the diagram, dark red solid frames denote thermodynamically stable structures, whereas dark red

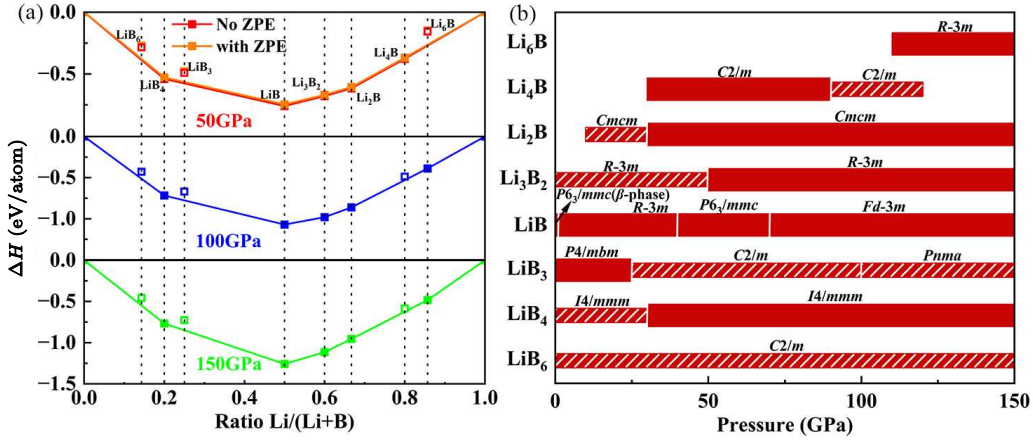


Fig. 1. Energetic stability of the Li–B system under pressure. (a) The calculated convex hulls for Li–B compounds at different pressures (50 GPa, 100 GPa, and 150 GPa). Solid and open symbols represent thermodynamically stable and metastable compounds, respectively. (b) Pressure–composition phase diagram of Li–B compounds. Dark red solid frames (dark red dotted frames) denote stable structures and thermodynamically metastable but dynamically stable structures, respectively.

dotted frames indicate thermodynamically metastable but dynamically stable structures. We note that although formation enthalpy calculations show that Li_6B lies on the convex hull at 100 GPa, indicating thermodynamic stability at this pressure, phonon dispersion calculations reveal the presence of imaginary modes, demonstrating that the *R-3m* Li_6B phase is dynamically unstable at 100 GPa. With increasing pressure, these imaginary modes are suppressed, and the phonon spectrum becomes fully stable above approximately 110 GPa. Therefore, Li_6B is identified as a stable phase in Fig. 1(b) only for pressures exceeding 110 GPa, where both thermodynamic and dynamical stability criteria are satisfied. The enthalpy–pressure relations for LiB and LiB_3, phonon dispersion calculations, the crystal structures, and the optimized lattice parameters and atomic positions are summarized in Figs. S1–S4 and Table S1.[58]

3.2. Electride Li_6B with superconducting and superionic behavior

Prompted by the lack of detailed studies on the electronic structure and dynamical behavior of Li_6B, and inspired by recent findings on electride, superconducting, and superionic behavior in lithium-rich compounds, we investigated the electron distribution, electronic properties, and dynamical behavior of Li_6B. Li_6B crystallizes in a hexagonal *R-3m* structure, where each B atom is coordinated with 18 neighboring Li atoms. This unique arrangement forms a cage-like framework consisting of two three-membered rings, six four-membered rings, and six five-membered rings (Fig. 2(a)).

To investigate the electronic properties of Li_6B, we calculated the electron localization function (ELF), partial charge density, electronic band structures, and partial density of states (PDOS). The ELF analysis revealed pronounced electron localization in the interstitial spaces, acting as interstitial quasi-atoms (ISQs) with a distinctive bone-shaped distribution (Fig. 2(a)), and Bader charge analysis further supports this conclusion (Table S3). As shown in Fig. 2(b), the orbital-projected band structure of Li_6B, calculated in the absence of spin–orbit coupling (SOC), shows a single band crossing the Fermi level (E_F), predominantly composed of Li and ISQ orbitals, indicative of metallic character. The PDOS analysis reveals a broad density-of-states peak around E_F primarily derived from Li-2p states, with strong orbital hybridization involving the bone-shaped ISQs, as shown in Fig. 2(b). Additionally, Fig. 2(c) illustrates the band-decomposed electron density maps within an energy window of 100 meV near E_F on the (−1 1 0) plane, displaying the bone-shaped distribution around the ISQs. This result suggests that electrical

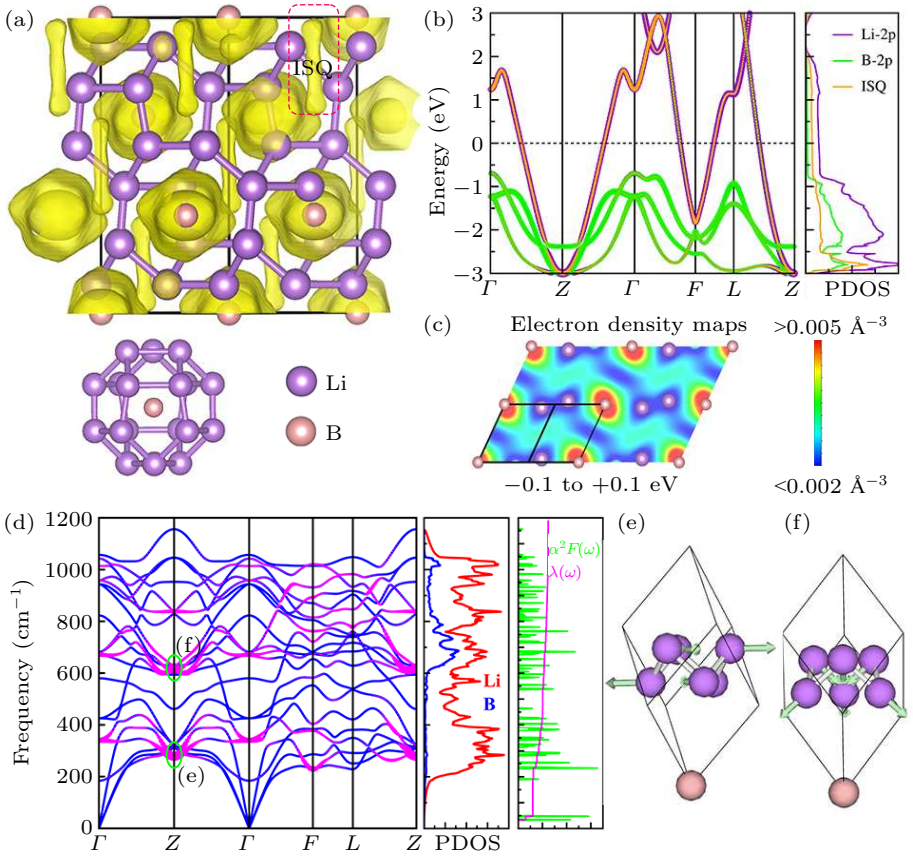


Fig. 2. Electronic and superconducting properties of *R-3m* Li_6B at 150 GPa. (a) The crystal structure and the ELF isosurface with a value of 0.8. (b) The band structures and PDOS. (c) Electron density maps within an energy window of 100 meV near the Fermi level. (d) Phonon band structures, projected density of states, Eliashberg spectral function, and the electron–phonon coupling constant λ. The sizes of the violet solid circles are proportional to the electron–phonon coupling strength. (e)–(f) The vibrational modes at the *Z* point.

conduction in Li_6B arises from both Li-derived electrons and anionic electrons confined within the interstitial space.

Encouraged by its metallic nature, we further investigated the superconductivity of *R-3m* Li_6B at a pressure of 150 GPa. To assess its superconducting potential, we employed density functional perturbation theory to calculate the electron–phonon (e–ph) coupling, phonon spectrum, partial phonon density of states (PHDOS), Eliashberg spectral function $\alpha^2F(\omega)$, and e–ph integral $\lambda(\omega)$. The superconducting transition temperature (T_c) is estimated using the Allen–Dynes modified McMillan equation

$$T_c = \frac{\omega_{\log}}{1.2}\exp\left[-\frac{1.04(1+\lambda)}{\lambda-\mu^*(1+0.62\lambda)}\right],$$

with the Coulomb pseudopotential μ^* of 0.1. Our results indicate that the cumulative e–ph coupling parameter λ is 1.42, a relatively large value for conventional superconductors, suggesting that Li_6B is a strong-coupling superconductor. PHDOS analysis shows that Li atoms dominate the entire frequency range, while B atoms contribute primarily to the high-frequency region (Fig. 2(d)). Specifically, the low-frequency range (0–300 cm^{-1}) and the intermediate-frequency range (300–600 cm^{-1}) contribute 42.0% and 34.1% to the total e–ph coupling parameter λ, respectively. The phonon spectrum reveals that the optical modes at the Z point soften, with large phonon linewidths, indicating strong coupling to the electrons. These modes mainly arise from vibrations of Li atoms (Figs. 2(e) and 2(f)). This interaction plays a key role in the superconductivity of Li_6B. The T_c of *R-3m* Li_6B is estimated to be around 51.0 K (Fig. 3), which is higher than that of other Li-rich superconducting electrides.[33,34,36–38,42–44,46,59–64]

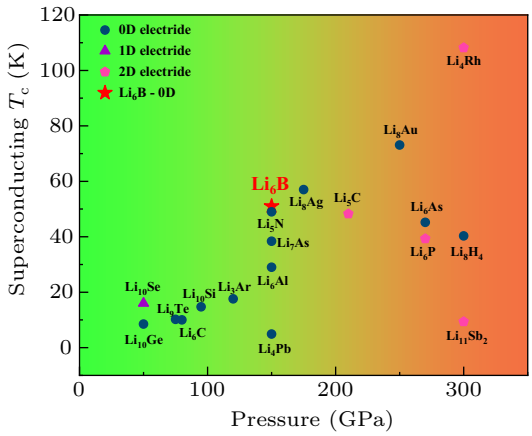


Fig. 3. Pressure-dependent superconducting transition temperature (T_c) diagrams for lithium-based electrides and the *R-3m* Li_6B phase (red star).

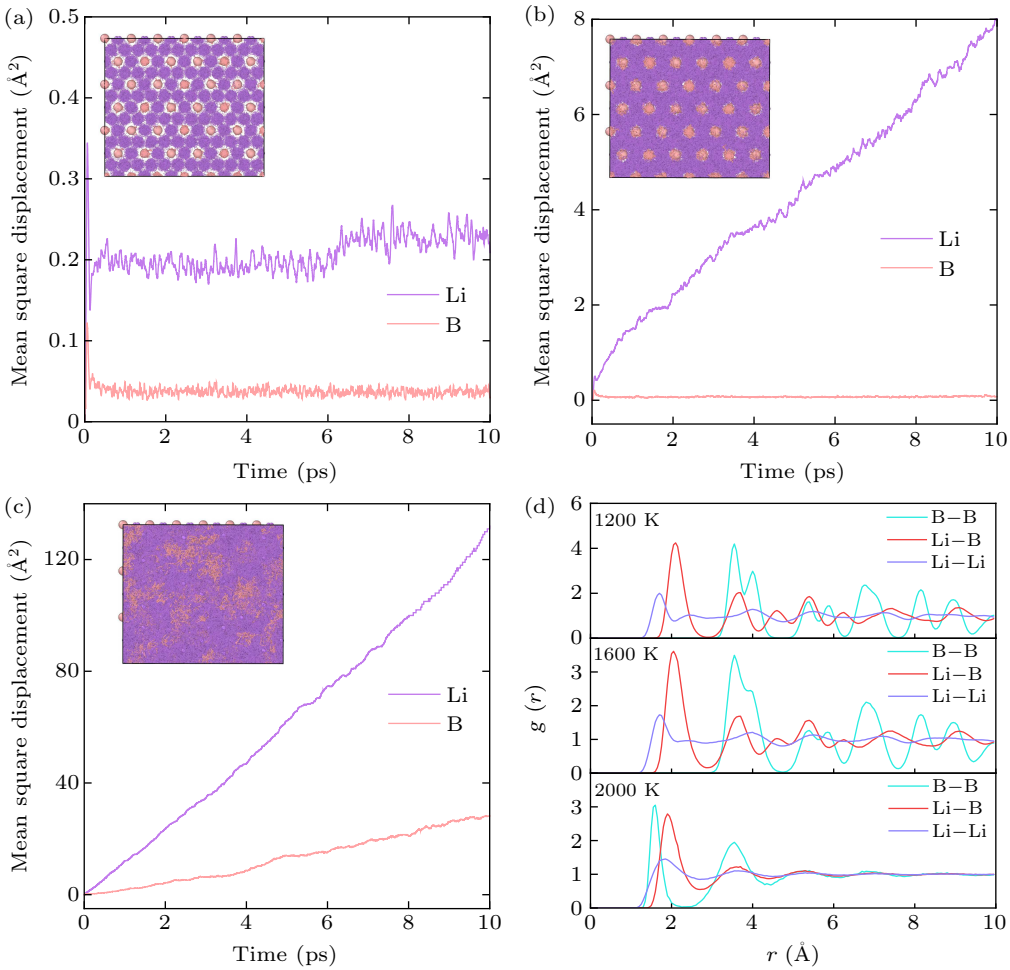


Fig. 4. Dynamical properties of *R-3m* Li_6B at 150 GPa. MSDs of Li and B atoms at (a) 1200 K (solid state), (b) 1600 K (superionic state), and (c) 2000 K (liquid state). (d) Pair distribution functions $g(r)$ between Li–Li, Li–B, and B–B at different temperatures.

We also investigated the dynamical behavior of *R-3m* Li_6B using AIMD simulations by calculating the mean-square displacements (MSD). All simulations began from the relaxed configuration at 150 GPa with varying temperatures. At 1200 K, the MSD of the atoms is minimal, indicating that all atoms remain confined to their equilibrium positions, preserving the solid state of Li_6B (Fig. 4(a)). As the temperature increases to 1600 K (Fig. 4(b)), the MSD of Li atoms increases rapidly, suggesting a transition to a superionic state. In this state, the sublattice of B atoms remains fixed, while Li atoms diffuse freely through the sublattice, with a diffusion coefficient of $D^{\mathrm{Li}} = 1.867 \times 10^{-5}$ cm^2·s^{-1}. Upon further heating the superionic phase to 2000 K, all atoms melt, transitioning to a fluid state (Fig. 4(c)). Additionally, we analyzed the atomic motions in Li_6B using radial distribution functions (RDFs) (Fig. 4(d)). At 1600 K, the Li–Li and Li–B partial RDFs exhibit more liquid-like behavior, while the B–B RDF remains solid-like. We attribute this behavior to the unique lightweight boron sublattice in Li_6B, which creates low-energy diffusion channels for lithium ions. Lithium ions migrate through vacancies or interstitial sites, typically driven by thermal excitation, enabling them to overcome energy barriers within the lattice.

3.3. Superconducting open-framework allotrope of boron at ambient pressure

LiB_6 has a monoclinic *C2/m* crystal structure, where cage-like units of B atoms are interspersed with Li atoms, forming a three-dimensional framework stacked along the *c* axis (Fig. 5(a)). *Ab initio* MD simulations demonstrate that the B_{12}-caged structure can be maintained at 100 K, 300 K, and 500 K at 0 GPa (Fig. S6). The orbital-projected band structure and partial density of states of LiB_6 at 0 GPa, shown in Fig. 5(b), reveal its metallic nature, with three bands crossing the Fermi level, primarily derived from B-p orbitals, particularly the B-p_y orbital. We also evaluated the superconducting properties of LiB_6, estimating the critical temperature (T_c) to be 22.1 K at 0 GPa, with an e–ph coupling constant λ of 1.02. As shown in Fig. 5(c), the phonon density of states indicates that low-frequency phonon modes below 300 cm^{-1}, associated with hybridization of Li and B atomic vibrations, contribute 43% to λ. It is worth noting that the optical mode at the Γ point ($\sim$ 500 cm^{-1}), with a large phonon linewidth, shown in Fig. 5(d), corresponds to vibrations of two layers of B atoms in the *ab* plane away from the Li layer.

Recent techniques for synthesizing allotropes of boron- and carbon-group elements using appropriate chemical precursors followed by physical and chemical manipulation have gained popularity.[65,66] For example, Sung *et al.*[67] reported a metallic *P6/m*-Si_6 phase obtained by removing Na from the novel Na–Si clathrate *P6/m*-$NaSi_6$ after pressure release. Similarly, Gu *et al.*[68] demonstrated that a single-layer T-graphite C_4 can be derived by evaporating K atoms. Inspired by these approaches, we propose that a new boron allotrope with a *C2/m* space group can be synthesized by removing Li atoms from LiB_6. As shown in Fig. 6(a), this removal prompts structural rearrangements within the three-dimensional open framework of boron atoms. The resulting boron structure consists of two distinct layers: the top layers form B_{14} caged structures, while the bottom layers consist of B_{16} cages.

We next investigate the electronic properties of *C2/m*-B_{12}, with its calculated band structure shown in Fig. 6(b). In the

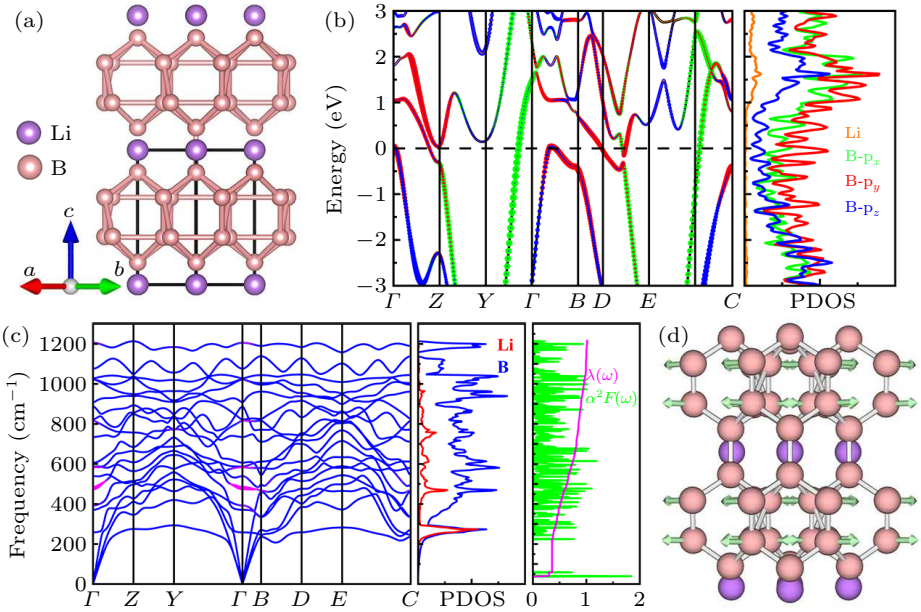


Fig. 5. Electronic and superconducting properties of *C2/m* LiB_6 at 0 GPa. (a) The crystal structure of *C2/m* LiB_6. (b) The electronic band structure and PDOS. (c) The calculated phonon dispersion curves, Eliashberg spectral functions together with the electron–phonon integral and PHDOS. (d) The vibrational mode at the Γ point.

absence of Li atoms, the Fermi level is lower compared to LiB_6, resulting in two bands crossing E_F. As shown in Fig. 6(b), the electronic density of states at the Fermi level is mainly derived from B-p_z orbitals. We also assess the superconducting properties through electron–phonon coupling calculations, estimating T_c to be approximately 21.4 K at ambient pressure. Figure 6(c) shows two optical modes at the Γ point with large phonon linewidths, which contribute significantly to the electron–phonon coupling constant. The vibrations of these modes are depicted in Fig. 6(d).

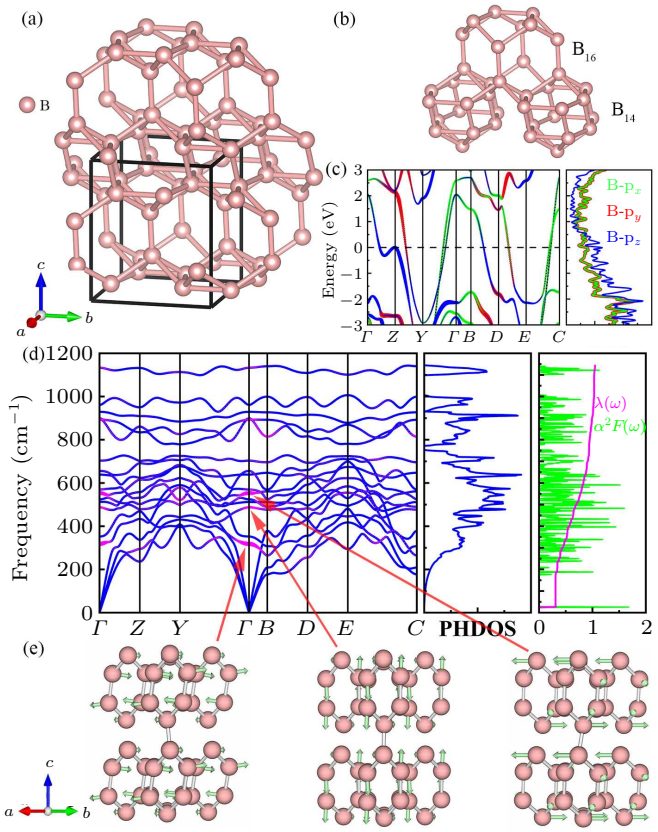


Fig. 6. Electronic and superconducting properties of *C2/m* B_{12} at 0 GPa. (a) The crystal structure of *C2/m* B_{12}. (b) The electronic band structure and PDOS. (c) The calculated phonon dispersion curves, Eliashberg spectral functions together with the electron–phonon integral and PHDOS. (d) The vibrational modes at the Γ point.

4. Conclusion

Through machine-learning-assisted crystal structure prediction and first-principles calculations, we found that the *R*-3m Li_6B compound is an electride, exhibiting a superconducting transition temperature of approximately 51 K at 150 GPa and transitioning to a superionic state at high temperatures. Additionally, we identified a metastable monoclinic $C2/m$ LiB_6 structure, which remains dynamically stable at ambient pressure, and discovered a metallic boron allotrope, $C2/m$-B_{12}, formed by removing Li from LiB_6. $C2/m$-B_{12} demonstrates a superconducting transition temperature of 21.4 K. These findings enhance our understanding of the electronic and structural behavior of lithium–boron systems under extreme conditions, while also opening new possibilities for applications of boron-based materials in high-performance electronics and energy devices.

Acknowledgments

This work was supported by the National Natural Science Foundation of China (Grant Nos. 12304022, T2495231, 12125404, 123B2049, and 52361035), the National Key R&D Program of China (Grant No. 2022YFA1403201), the Natural Science Foundation of Ningxia Hui Autonomous Region of China (Grant No. 2024AAC03014), the Basic Research Program of Jiangsu (Grant Nos. BK20233001 and BK20241253), the Jiangsu Funding Program for Excellent Postdoctoral Talent (Grant Nos. 2024ZB002 and 2024ZB075), the Postdoctoral Fellowship Program of CPSF (Grant No. GZC20240695), the AI & AI for Science program of Nanjing University, and the Fundamental Research Funds for the Central Universities. The calculations were carried out using supercomputers at the School of Physics and the High-Performance Computing Center of the Collaborative Innovation Center of Advanced Microstructures at Ningxia University, and the high-performance supercomputing center of Nanjing University.

References

[1] Olinger B and Shaner J W 1983 *Science* **219** 1071
[2] Hanfland M, Christensen N E and Novikov D L 2000 *Nature* **408** 174
[3] Guillaume C L, Gregoryanz E, Degtyareva O, McMahon M I, Hanfland M, Evans S, Guthrie M, Sinogeikin S V and Mao H K 2011 *Nat. Phys.* **7** 211
[4] Lv J, Wang Y, Zhu L and Ma Y 2011 *Phys. Rev. Lett.* **106** 015503
[5] Frost M, Kim J B, McBride E E, Peterson J R, Smith J S, Sun P and Glenzer S H 2019 *Phys. Rev. Lett.* **123** 065701
[6] Wang X, Wang Z, Gao P, Zhang C, Lv J, Wang H, Liu H, Wang Y and Ma Y 2023 *Nat. Commun.* **14** 2924
[7] Shimizu K, Takao D, Yagi T and Amaya K 2002 *Nature* **419** 597
[8] Struzhkin V V, Eremets M I, Gan W, Mao H K and Hemley R J 2002 *Science* **298** 1213
[9] Deemyad S and Schilling J S 2003 *Phys. Rev. Lett.* **91** 167001
[10] Matsuoka T and Shimizu K 2009 *Nature* **458** 186
[11] Marques M, McMahon M I, Gregoryanz E, Hanfland M, Guillaume C L, Pickard C J, Ackland G J and Nelmes R J 2011 *Phys. Rev. Lett.* **106** 095502
[12] Wang Y, Wang J, Hermann A, Pan S, Shi J, Wang H T, Xing D and Sun J 2022 *Phys. Rev. B* **105** 214101
[13] Yao Y, Tse J S and Klug D D 2009 *Phys. Rev. Lett.* **102** 115503
[14] Pickard C J and Needs R J 2009 *Phys. Rev. Lett.* **102** 146401
[15] Tamblyn I, Raty J Y and Bonev S A 2008 *Phys. Rev. Lett.* **101** 075703
[16] Schaeffer A M J, Talmadge W B, Temple S R and Deemyad S 2012 *Phys. Rev. Lett.* **109** 185702
[17] Lazicki A, Fei Y and Hemley R J 2010 *Solid State Commun.* **150** 625
[18] Albert B and Hillebrecht H 2009 *Angew. Chem. Int. Ed.* **48** 8640
[19] Li X B, Xie S Y, Zheng H, Tian W Q and Sun H B 2015 *Nanoscale* **7** 18863
[20] Han W H, Oh Y J, Choe D H, Kim S, Lee I H and Chang K J 2017 *NPG Asia Mater.* **9** e400
[21] Nagamatsu J, Nakagawa N, Muranaka T, Zenitani Y and Akimitsu J 2001 *Nature* **410** 63
[22] Vuong T Q P, Liu S, Van der Lee A, Cuscó R, Artús L, Michel T, Valvin P, Edgar J H, Cassabois G and Gil B 2018 *Nat. Mater.* **17** 152
[23] Li Y, Hao J, Liu H, Lu S and Tse J S 2015 *Phys. Rev. Lett.* **115** 105502
[24] Zhang S, Du X, Lin J, Bergara A, Chen X, Liu X, Zhang X and Yang G 2020 *Phys. Rev. B* **101** 174507

[25] Dye J L 2003 *Science* **301** 607

[26] Pickard C J and Needs R J 2011 *Phys. Rev. Lett.* **107** 087201

[27] Kitano M, Inoue Y, Yamazaki Y, Hayashi F, Kanbara S, Matsuishi S, Yokoyama T, Kim S W, Hara M and Hosono H 2012 *Nat. Chem.* **4** 934

[28] Hu J, Xu B, Yang S A, Guan S, Ouyang C and Yao Y 2015 *ACS Appl. Mater. Interfaces* **7** 24016

[29] Wu J, Gong Y, Inoshita T, Fredrickson D C, Wang J, Lu Y, Kitano M and Hosono H 2017 *Adv. Mater.* **29** 1700924

[30] Hirayama M, Matsuishi S, Hosono H and Murakami S 2018 *Phys. Rev. X* **8** 031067

[31] Park C, Kim S W and Yoon M 2018 *Phys. Rev. Lett.* **120** 026401

[32] Huang H, Jin K H, Zhang S and Liu F 2018 *Nano Lett.* **18** 1972

[33] Liu Z, Zhuang Q, Tian F, Duan D, Song H, Zhang Z, Li F, Li H, Li D and Cui T 2021 *Phys. Rev. Lett.* **127** 157002

[34] Zhao Z, Zhang S, Yu T, Xu H, Bergara A and Yang G 2019 *Phys. Rev. Lett.* **122** 097002

[35] Hou J, Dong X, Oganov A R, Weng X J, Hao C M, Yang G, Wang H T, Zhou X F and Tian Y 2022 *Phys. Rev. B* **106** L220501

[36] Guo Z, Bergara A, Zhang X, Li X, Ding S and Yang G 2024 *Phys. Rev. B* **109** 134505

[37] Zhang X, Yao Y, Ding S, Bergara A, Li F, Liu Y, Zhou X F and Yang G 2023 *Phys. Rev. B* **107** L100501

[38] Wang Q, Wei J, Zhong T, Sun J, Gao B, Zhu L, Liu H and Zhang S 2024 *Phys. Rev. B* **110** 144523

[39] Cavazzoni C, Chiarotti G L, Scandolo S, Tosatti E, Bernasconi M and Parrinello M 1999 *Science* **283** 44

[40] Gao H, Liu C, Shi J, Pan S, Huang T, Lu X, Wang H T, Xing D and Sun J 2022 *Phys. Rev. Lett.* **128** 035702

[41] Hernandez J A, Bethkenhagen M, Ninet S, French M, Benuzzi-Mounaix A, Datchi F, Guarguaglini M, Lefevre F, Occelli F and Redmer R 2023 *Nat. Phys.* **19** 1280

[42] Wang X, Wang Y, Wang J, Pan S, Lu Q, Wang H T, Xing D and Sun J 2022 *Phys. Rev. Lett.* **129** 246403

[43] Wan Z, Xu W, Yang T and Zhang R 2022 *Phys. Rev. B* **106** L060506

[44] Lu Q, Ding C, Jia Q, Pan S, Shi J, Han Y, Wang J, Wang X, Xing D and Sun J 2024 *Phys. Rev. B* **109** L180507

[45] Zhang Z, Lu Q, Ding C, Huang T, Zhu Y, Han Y, Wang J, Wang X and Sun J 2024 *Phys. Rev. B* **110** 174101

[46] Wang Q, Cui W, Xu W, Gao K, Hao J, Shi J, Liu H and Li Y 2024 *Phys. Rev. B* **110** 134114

[47] Zhou P, Ni Y, Wang J, Han Y, Li Y, Lu Q, Zhang Z, Wang X and Sun J 2025 *Phys. Rev. B* **111** 134109

[48] Xia K, Gao H, Liu C, Yuan J, Sun J, Wang H T and Xing D 2018 *Sci. Bull.* **63** 817

[49] Wang J, Gao H, Han Y, Ding C, Pan S, Wang Y, Jia Q, Wang H T, Xing D and Sun J 2023 *Natl. Sci. Rev.* **10** nwad128

[50] Perdew J P, Burke K and Ernzerhof M 1996 *Phys. Rev. Lett.* **77** 3865

[51] Blöchl P E 1994 *Phys. Rev. B* **50** 17953

[52] Kresse G and Furthmüller J 1996 *Phys. Rev. B* **54** 11169

[53] Giannozzi P, Baroni S, Bonini N, Calandra M, Car R, Cavazzoni C, Ceresoli D, Chiarotti G L, Cococcioni M and Dabo I 2009 *J. Phys. Condens. Matter* **21** 395502

[54] Nosé S 1984 *J. Chem. Phys.* **81** 511

[55] Grest G S and Kremer K 1986 *Phys. Rev. A* **33** 3628

[56] Peng F, Miao M, Wang H, Li Q and Ma Y 2012 *J. Am. Chem. Soc.* **134** 18599

[57] Hermann A, McSorley A, Ashcroft N W and Hoffmann R 2012 *J. Am. Chem. Soc.* **134** 18606

[58] Supplemental Material

[59] Zhang X, Zhao Y, Bergara A and Yang G 2022 *J. Chem. Phys.* **156** 194112

[60] Zhang X, Li F, Bergara A and Yang G 2021 *Phys. Rev. B* **104** 134505

[61] Li X, Hermann A, Peng F, Lv J, Wang Y, Wang H and Ma Y 2015 *Sci. Rep.* **5** 16675

[62] Wan Z, Zhang C, Yang T, Xu W and Zhang R 2022 *New J. Phys.* **24** 113012

[63] Zhao Y, Bergara A, Zhang X, Li F, Liu Y and Yang G 2023 *Phys. Rev. B* **108** 104505

[64] Pereira Z S, Faccin G M and da Silva E Z 2021 *J. Phys. Chem. C* **125** 8899

[65] Gryko J, McMillan P F, Marzke R F, Ramachandran G K, Patton D, Deb S K and Sankey O F 2000 *Phys. Rev. B* **62** R7707

[66] Stefanoski S, Malliakas C D, Kanatzidis M G and Nolas G S 2012 *Inorg. Chem.* **51** 8686

[67] Sung H J, Han W H, Lee I H and Chang K J 2018 *Phys. Rev. Lett.* **120** 157001

[68] Gu Q, Xing D and Sun J 2019 *Chin. Phys. Lett.* **36** 097401